Interaction of Cationic Colloids at the Surface of J774 Cells: A Kinetic Analysis

Pascale Chenevier,* Bernard Veyret,† Didier Roux,* and Nelly Henry-Toulmé*
*Centre de Recherche Paul Pascal, CNRS, 33600 Pessac, France, and †Laboratoire de Physique des Interactions Ondes Matière, ENSCPB BP 108, 33402 Talence Cedex, France

ABSTRACT We have characterized the binding of multilamellar colloids to J774 cells. Cationic colloids were shown to bind much more efficiently than neutral ones. Particle uptake by cells was followed by flow cytometry and fluorescence microscopy. Analysis of the kinetics of uptake of cationic particles indicated that binding on the cell surface occurred with two characteristic times. Analysis of the dissociation properties allowed discriminating between several alternative models for adsorption and led us to propose a mechanism that involved two independent classes of binding sites on the cell surface. One class of sites appeared to be governed by a classic mass action law describing a binding equilibrium. The other sites were populated irreversibly by particles made of 10% cationic lipids. This was observed in the absence of endocytosis, under conditions where both the equilibrium and the irreversible binding occurred at the cell surface. We determined the rate constants for the different steps. We found that the reversible association occurred with a characteristic time of the order of tens of seconds, whereas the irreversible binding took a hundred times longer. The presence of serum proteins in the incubation medium did not drastically affect the final uptake of the particles. In contrast, the capture of the particles by cells significantly dropped when the fraction of positively charged lipids contained in the colloids was decreased from 10% to 5%. Finally, the results will be discussed within a comprehensive model where cationic particles find labile binding sites in the volume of the pericellular network (glycocalyx and extracellular matrix) and less-accessible irreversible binding sites at the cell membrane itself.

INTRODUCTION

The way cells communicate with their environment, through chemical, electric, or mechanical signals, is highly sophisticated and regulated. Nevertheless, the whole process leading to signal transmission and cell response usually involves an initial and limiting step that entails some sort of recognition at the cell surface. Most common mechanisms for such recognition require specific binding of ligands (sugars, proteins, lectins, etc.) to membrane receptors (proteins). This type of key-lock interaction also determines cell-cell adhesion and tissue architecture, and certainly represents one of the principal bases of cell functioning. However, how cells capture "untagged" objects such as particles devoid of specific recognition molecules remains unclear. Scientists who attempted to use colloidal systems as drug carriers and delivery vehicles (Poste and Papahadjopoulos, 1978; Benita and Levy, 1993; Kreuter, 1994) have addressed this question for years. Mainly, liposomes and, to a lesser extent, polymer particles, have been considered. Because of the nature of the components of these particles (natural lipids and biodegradable polymers), essentially neutral and anionic objects have been used, leading to the emergence of some guidelines. In vivo, the whole fate of the particles is dominated by their interactions with serum proteins (Bonté and Juliano, 1986; Scherphof et al., 1981; Kamps et al., 1999; Roerdink et al., 1983). The grafting on the particle surface of hydrophilic polymers such as polyethyleneglycol (stealth liposomes) significantly reduces protein adsorption and thus clearance of the particles by the cells of the reticuloendothelial system (Papahadjopoulos et al., 1991; Woodle and Lasic, 1992; Allen and Hansen, 1991; Allen et al., 1992). In vitro, the presence of specific ligands on the surface of the particles typically enhances uptake of the particles by the cells (Leserman et al., 1981; Park et al., 1995; Henry-Toulmé et al., 1995; Goren et al., 1996; Kirpotin et al., 1997; Meyer et al., 1998). Nevertheless, negatively charged particles appear to be more efficiently captured by cells than neutral ones, although several orders of magnitude less efficiently than specifically targeted objects (Allen et al., 1988; Lee et al., 1992; Miller et al., 1998). Very little is known about cationic particles (Miller et al., 1998; Pires et al., 1999) except for their increasing interest in the field of nucleic acids packaging for cells transfection and gene therapy. Indeed, a new class of colloids has recently been described, made by molecular assembling of DNA or RNA chains condensed with polycations such as lipid aggregates (Schwartz et al., 1995; Hofland et al., 1996; Koltover et al., 1998, Yang and Huang, 1998), peptides (Legendre et al., 1995, 1997; Wadhwa et al., 1997; Dufourcq et al., 1998), or polymers (Legendre et al., 1993; Haensler and Szoka, 1993; Boussif et al., 1996; Gao and Huang, 1996; Erbacher et al., 1999). The electrostatic complexes formed during such condensation constitute a colloidal suspension of hybrid particles with physicochemical properties (size, zeta potential, stability, etc.) that de-

Received for publication 16 December 1999 and in final form 24 May 2000.

Address reprint requests to Dr. Nelly Henry-Toulmé, Centre de Recherche Paul Pascal, CNRS, Avenue A. Schweitzer, F-33600 Pessac, France. Tel.: 33-556-84-56-21; Fax: 33-556-84-56-00; E-mail: henry@crpp.u-bordeaux.fr

0006-3495/00/09/1298/12 $2.00

pend on the nature of the cations and the preparation conditions. Some of these complexes, prepared in the presence of an excess of positive charges, successfully transfected cells in vitro.

In this paper we present a thermodynamic analysis of the interactions of cationic colloids with the cell surface in vitro. This work was aimed at gaining insight into the mechanism of these interactions, not only because of the interest of such entities in gene therapy but also because they may supply tools for exploring the type of organization selected by cells to sort the "untagged" particles.

We investigated this question using biocompatible colloids flexible as regard to their formulation, with a mean size compatible with a potential internalization. We focused our attention on the adhesion step and concentrated our experiments on cationic colloids. We explored both the binding and the kinetics of the process. The analytical solutions that we derived to model our data prompted us to suggest an adhesion mechanism that involved two independent steps. This model will be discussed in the light of previous results obtained by other authors for neutral and anionic particles. The influence of serum proteins, temperature, and charge density on the adhesion characteristics was also examined.

MATERIALS AND METHODS

Phosphatidyl choline purified from soybean lecithin (S100) was purchased from Lipoid GmbH (Ludwigshafen, Germany), tetraethylenglycol mono *n*-dodecylether (Lauropal) from Nikko Chemicals Co. (Tokyo, Japan), and dioleyltrimethylammonium propane (DOTAP) from Avanti Polar Lipids (Birmingham, AL). Calcein was purchased from Sigma (St. Louis, MO) and used without further purification. Transferrin, from human serum, fluorescein-conjugated, was purchased from Molecular Probes (Eugene, OR).

MLVs

The multilamellar colloids were prepared as already described (Diat et al., 1993), by shearing in a Couette cell, a homogeneous lamellar phase made of lipids and water. This produced a thick viscoelastic material composed of close-packed sealed multilamellar spheres structured like onions. The size profile had a main peak around 200–300 nm with a wide shoulder toward larger sizes, up to a few micrometers. The volume fraction occupied by the spheres in this paste was close to one and almost all the aqueous volume was trapped within the spheres in between the lamella. In our experiments, the spheres were made of 51% (w/w) phosphatidylcholine, 4% (w/w) Lauropal, and 50% (w/w) water. To obtain cationic spheres, from 2 to 10% of soybean lecithin was replaced by DOTAP. Fluorescent MLVs were obtained by replacing water with a 2×10^{-3} M calcein aqueous solution. Before use, the paste was dispersed 10 times in water and passed through 200-nm polycarbonate filters to narrow the size distribution, which was finally found centered at 230 ± 60 nm. This last step was confirmed not to significantly alter the MLV's concentration (inorganic phosphate was measured as in Hallen (1980)) or the calcein trapping efficiency. The untrapped calcein fraction was evaluated by the cobalt chloride fluorescence quenching method (Kendall and McDonald, 1983). The calcein trapping efficiency was always found around 75%. We verified by the same fluorescence method that calcein trapping remained stable over the time of our experiments. The particle concentration was calculated from the mean size and volume fraction. It was found equal to 2×10^{16} particles/l in the filtered suspension.

Cell culture and treatments

The J774 cells were cultured in suspension in Dulbecco's Modified Eagle's medium (DMEM) supplemented with 10% fetal calf serum. The cultures formed small aggregates easily dispersed by pipetting. For incubation with MLVs, cells were washed in phenol-red-free DMEM, always supplemented with 25 mM final concentration HEPES buffer. Incubation of the particles with the cells was performed in the absence of fetal calf serum except when specifically stated. The cell concentration was adjusted to 5×10^5 cells/ml. The MLVs were then added at the desired concentration under precisely controlled temperature conditions and regularly gently stirred to avoid significant sedimentation of the cells. After the appropriate incubation time, the cells were analyzed either by fluorescence microscopy or by flow cytometry without any further treatment.

Fluorescence microscopy

Fluorescence microscopy was performed using a Nikon Diaphot TMD inverted microscope equipped with the following filter set for calcein detection: blue excitation BP 450 to 490; LP 515. Images were collected through a Hammatsu CCD camera interfaced with a Matrox Meteor-II frame grabber. For observation, cells were allowed to settle on glass coverslips mounted in 35-mm petri dishes.

Flow cytometry

Experiments were performed using a Facscan cytometer (Becton-Dickinson) equipped with an argon laser. The sample was thermostated using a home-made device connected to a thermostated circulating bath (Ministat, Huber, Rimsting, Germany). At least 4000 events were counted at 60 μl/min for each point. The software package Cell Quest (Becton-Dickinson, Le Pont de Claix, France) was used to determine the events of interest from forward and side scatter parameters. The mean fluorescence intensity of the cells was obtained from the mean channel number of the fluorescence histograms of the gated population.

Data analysis

The data have been adjusted to the analytical expression using the Levenberg-Marquardt algorithm. Errors are mean standard deviations of at least three independent experiments.

RESULTS

Binding of positively charged versus neutral MLVs

J774 cells were incubated with cationic MLVs (10% positive lipids). Their zeta potential in water was found equal to +50 mV. In parallel, the same experiment was conducted with MLVs made of neutral lipids only and having a zeta potential in water equal to −20 mV. The fluorescence retained by cells after 2 h incubation with increasing concentrations of these cationic or neutral particles loaded with calcein was measured by flow cytometry at 25°C. Fig. 1 shows the scattering plots and fluorescence histograms obtained on cell populations treated with 2×10^{14} particles/l.

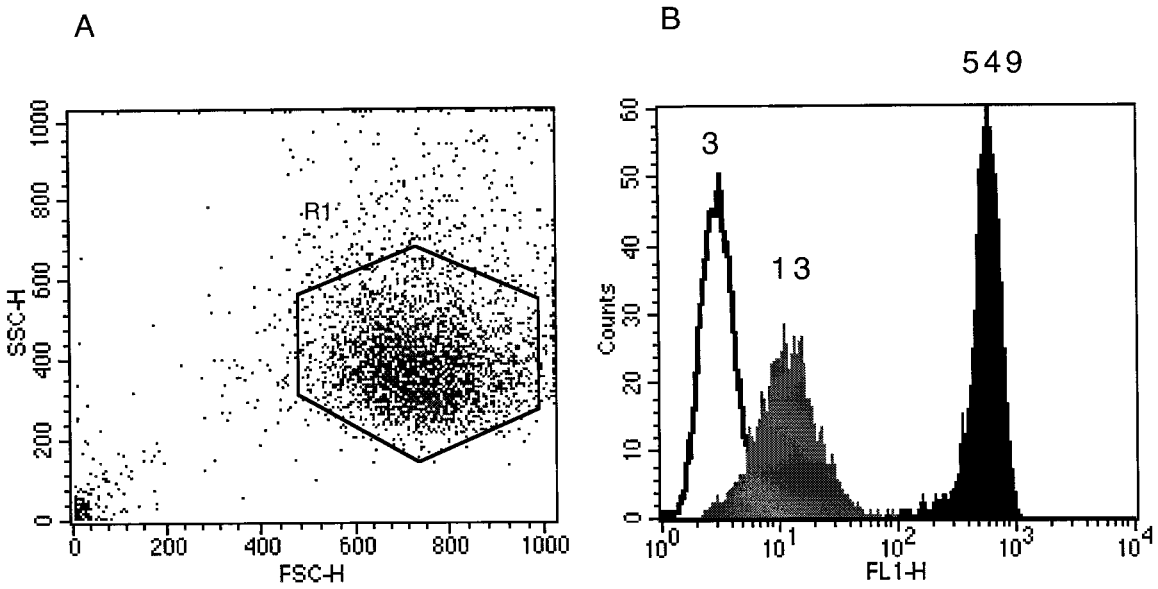

FIGURE 1 Scattering plot and fluorescence histograms of J774 cells incubated with particles. The scattering plot (*A*) gives forward scattering (FSC-H) versus side scattering (SSC-H) for each event; 4000 events were counted per sample. Only events having the FSC and SSC couple of values comprising area R1 were taken into consideration for fluorescence analysis. Similar scattering plots were obtained with or without particles and whatever nature of the particles. (*B*) shows the fluorescence intensity histograms obtained with cells incubated for 2 h in the presence of unlabeled neutral (*open histogram*), calcein-loaded neutral (*gray histogram*) and calcein-loaded cationic, i.e., containing 10% DOTAP (*filled histogram*) particles. Particle concentration was equal to 2×10^{14} particles./l. The numbers on the histograms represent mean fluorescence value of the distribution.

Only cationic particles induced high levels of fluorescence, while the fluorescence histogram obtained with neutral particles at the same concentration was very close to the one obtained with untreated cells. In either case, the fluorescence distribution was mainly contained in a single narrow peak, indicating a homogeneous cell response to the particles over the entire population. Cell labeling (mean value of the fluorescence distribution) was then studied as the particle concentration was increased. When cells received cationic MLVs, the fluorescence signal increased with particle concentration and reached a plateau (Fig. 2). In contrast, the fluorescence signal obtained with neutral particles increased linearly, as when cells were treated with identical concentrations of free calcein (Fig. 2). This indicated that free calcein was able to partition within the cells proportionally to its concentration. However, the calcein trapping efficiency values measured by the Co^{2+}-quenching method on the MLV preparation indicated that $15 \pm 5\%$ of free calcein was added together with the labeled particles. This led us to the conclusion that the fluorescence retained by cells treated with neutral particles corresponded to the background produced by the small fraction of free calcein. This was confirmed by fluorescence microscopy observations (Fig. 3). Bright spots could be visualized on cells brought into contact with cationic particles (Fig. 3 *D*), whereas only a faint diffuse fluorescence was observed on cells treated with neutral particles (Fig. 3 *B*), supporting the idea that the cells did not trap any of the latter particles. At that point, it appeared clearly that the presence of 10% of cationic molecules on the surface of the colloid induced significant binding to J774 cells cultured in suspension, and that this binding could be precisely quantified by flow cytometry.

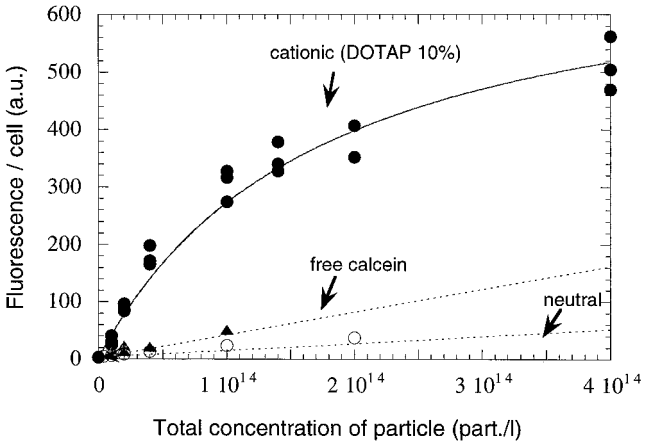

FIGURE 2 Binding of particles on J774 cells measured by flow cytometry. Cells were treated at 25°C for 2 h with increasing concentrations of calcein-loaded particles, neutral (○), and cationic (●), i.e., containing 10% DOTAP particles. Mean fluorescence per cell was also measured in cells treated with equivalent concentrations of free calcein (▲). All measurements were done in the absence of proteins. Cell concentration was equal to 5×10^5/ml. The calculated line corresponds to a fit according to the expression $y = m_1 (m_2x/1 + m_2x)$ with $m_1 = 739$ and $m_2 = 1.7 \times 10^{14}$ M^{-1}.

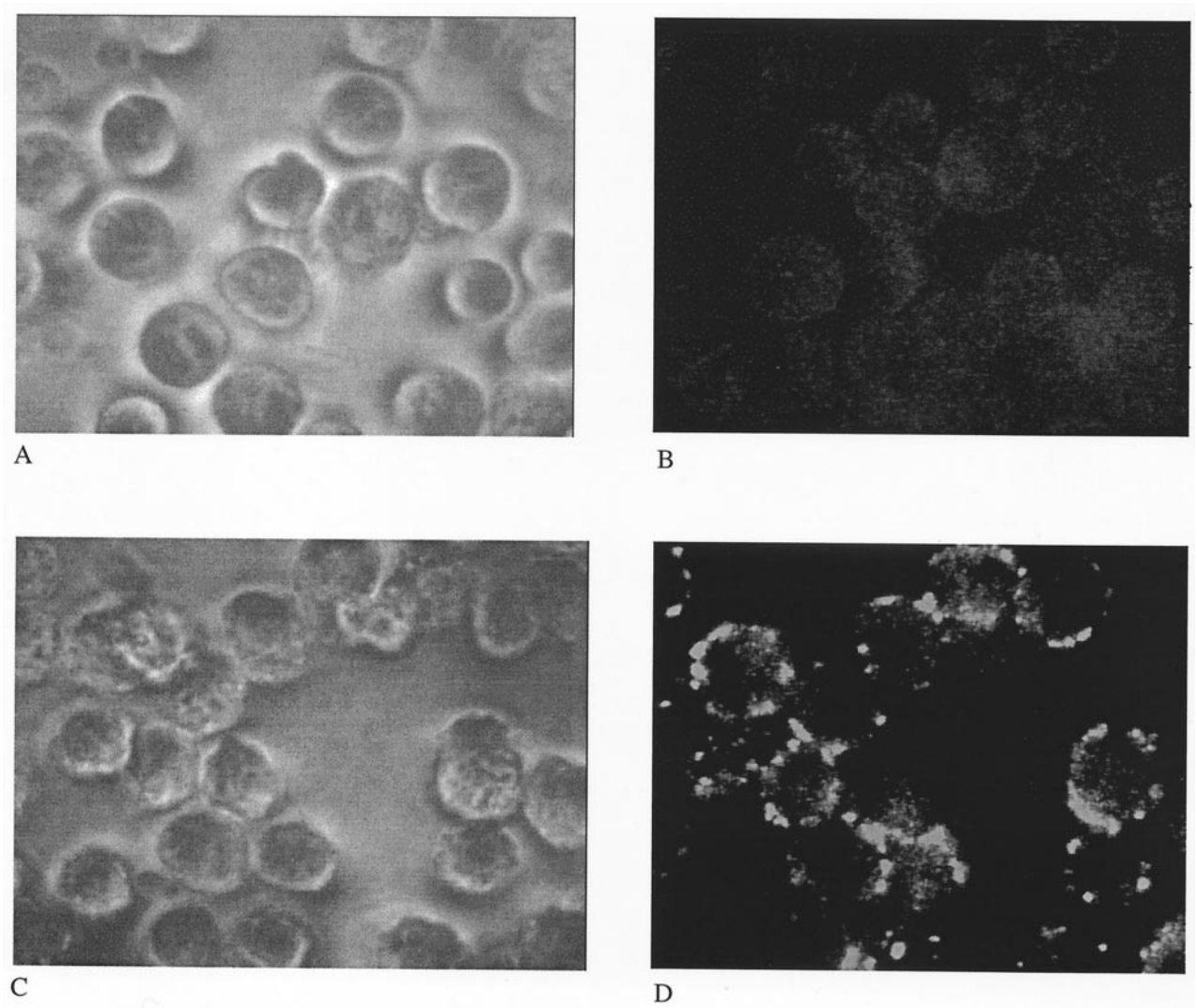

FIGURE 3 Capture of particles by J774 cells. Phase contrast (*A, C*) and fluorescence images (*B, D*) of J774 cells treated for 2 h with calcein-loaded neutral (*A, B*) or cationic (*C, D*), i.e., containing 10% DOTAP particles. Particle concentration was equal to 2×10^{14} particles/l.

Therefore, it was possible to investigate the mechanism of the binding. The shape of the curve in Fig. 2, giving the amount of bound particles as a function of the total particle concentration, strongly evoked Langmuir adsorption equilibrium. It could be fit to an expression of the form of the type $y = m_1 (m_2x/1 + m_2x)$, where x represents the particle molar concentration, m_1 the saturating amount of bound particles and m_2 the adsorption constant K. However, this assumes a priori that only one class of binding sites is populated through a simple equilibrium. We thus decided to explore the binding process from the kinetic point of view to better elucidate the mechanism involved in particle capture by the cells.

Kinetics of cationic spherulite adsorption

The kinetics of cationic spherulite binding was first assessed at low temperature (4°C) in order to distinguish the binding at the surface from any other process such as internalization by an endocytic process. Using fluorescence microscopy, we made sure that the particles remained located at the cell surface under these conditions. The results obtained at 4°C with cationic MLVs containing 10% DOTAP are shown in Fig. 4. This curve gives the amount of fluorescence $F(t)$ retained by one cell (mean value over a 4000-cell population) at time t. It can be related to the molar concentration of bound particles as follows: $x(t) = n_o (F(t)/F_{max,\infty})$, where n_o is the total initial molar concentration of all binding sites; $n_o = Cs/A$, where C is the total cell concentration (cells/liter), s the number of binding sites per cell, and A Avogadro's number. In the above equation, $F_{max,\infty}$ is the mean fluorescence per cell measured at saturating concentrations of particles. An analytical expression was sought to fit the data shown in Fig. 4. Two characteristic times were required to obtain a satisfying fitting function. The simplest function

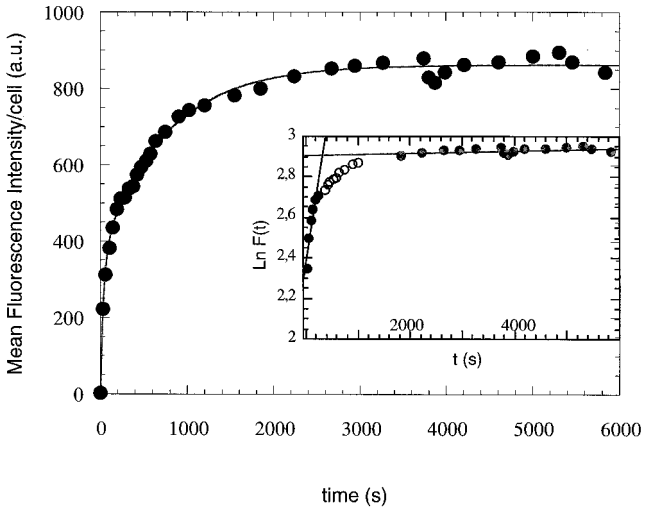

FIGURE 4 Kinetics of capture of cationic particles by J774 cells. Mean fluorescence, calculated for each point from a 4000-event fluorescence histogram, is given as a function of incubation time. 5×10^5 cell/ml were added at time $t = 0$ with 2×10^{14} particles/l. The temperature was set at 4°C. The solid line gives the fit of the experimental points (●) following the analytical expression $x(t) = m_1\ (1 - m_2e^{-m_3t} - (1 - m_2)e^{-m_4t})$. The *inset* shows the logarithmic representation of the same data.

was of the following form:

$$x(t) = m_1(1 - m_2e^{-m_3t} - (1 - m_2)e^{-m_4t}) \qquad (1)$$

Few mechanisms have kinetic equations following this expression. They are gathered in Table 1. The kinetic equations have been established for each mechanistic scheme by writing the differential expression of the bound particle concentration dx/dt as a function of the initial concentrations N_o and n_o, and of the various rate constants (see Appendix). To conveniently integrate these expressions, we made the approximation that the free particle fraction was constant and equal to the total concentration N_o, which also implies that x, the concentration of bound particles, was always negligible with respect to N_o. This approximation was checked experimentally: centrifugation experiments were performed to estimate the fraction of bound particles. Cell samples were treated with increasing concentrations of cationic MLVs (10% DOTAP) for 2 h and centrifuged to pellet the cells. The supernatants were collected and the amount of fluorescence was measured by spectrophotometry. Similar samples were prepared in the absence of cells to provide a total concentration reference. The results showed that the proportion of bound particles was low (<1%) and could not be determined by measuring the difference between total and unbound concentrations. This validates the approximation $N_o \gg x$ used to write the equations presented in Table 1.

Processes **a, b,** and **c** (see Table 1) involve two classes of independent binding sites n_1 and n_2 or n_a and n_i. Each could be populated independently through two different equilibria, or irreversible binding reactions. In all cases, two classes of bound species x_1 and x_2 should be produced and we should experimentally measure a quantity x, which is the sum of x_1 and x_2. In process **d** only one class of sites exists, but in two different states: the sites n are first populated according to an equilibrium, providing a reversibly bound particle z. This particle z, once bound, moves with a rate constant k_i to the state of an irreversibly bound particle y according to scheme **d.** In this case, we experimentally measure the sum of reversibly and irreversibly bound particles $x(t) = z(t) + y(t)$.

All processes listed above were described by kinetic equations of the same form (1) and were thus in agreement with the experimental curve with regard to the association of the particle with the cells. We therefore, needed additional criteria to discriminate between these four processes. To this purpose, we examined which particle dissociation profile could be expected from each process that had been selected by the association behavior.

Kinetics of cationic spherulite desorption

In case **a** the two types of bound species should be released upon washing according to two exponential decays $e^{-k_{d1}t}$ and $e^{-k_{d2}t}$. The repopulating of the free sites through k_{a1} and k_{a2} should be negligible, since N becomes small after washing: the effective constant being k_aN. In case **b,** no release should occur because irreversible binding reactions have been postulated. In case **c,** only a fraction $n_e/(n_e + n_i)$, bound reversibly in equilibrium, should be released exponentially with a characteristic time k_d.

In case **d,** the particles bound in state z could be released. The variation of their concentration with time has been calculated from the expression $z(t)$. The amount of reversibly bound particles rapidly increases to a maximum value depending on k_a and decays to zero depending on k_d and k_i. The profile of the dissociation upon washing should, in this case, parallel this time-dependence.

Thus, the four models have different dissociation profiles. Therefore, we designed experiments to follow the time dependence of the dissociation. During the incubation of the cells with the particles, samples were taken at various times within the first 2 h. The withdrawn samples were quickly centrifuged, resuspended in fresh buffer, and analyzed using the cytometer to measure the detachment kinetics. The fluorescence signal per cell decreased with a time-dependence that is shown in Fig. 5 for the sample taken up at time 2200 s (longest time examined). The dissociation profile seemed to follow a monoexponential decay with a value of k_d equal to 0.0087 s^{-1}. This value, however, was rather approximate because the time when dissociation was triggered was difficult to determine with accuracy, and also because the washing procedure did not allow the collection of data within the first 2 min of the dissociation. Most decisive was the variation of the amplitude of the fluores-

TABLE 1 Binding models predicting binding kinetics described by the equation $x(t) = m_1\,(1 - m_2e^{-m_3t} - m_34e^{-m_5t})$

a	$N + n_1 \underset{k_{d1}}{\overset{k_{a1}}{\rightleftarrows}} x_1$ $N + n_2 \underset{k_{d2}}{\overset{k_{a2}}{\rightleftarrows}} x_2$	$x(t) = x_1(t) + x_2(t) = \eta_o \cdot \eta_{12}\left[1 - \frac{n_{o1}}{n_o}\cdot\frac{1}{\eta_{12}}\cdot L_1\cdot e^{-\kappa_1 t} - \left(1 - \frac{n_{o1}}{n_o}\right)\cdot\frac{1}{\eta_{12}}\cdot L_2\cdot e^{-\kappa_2 t}\right]$ $\kappa_1 = k_{a1}N_o + k_{d1} \quad \kappa_2 = k_{a2}N_o + k_{d2}$ $L_1 = \frac{k_{a1}N_o}{k_{a1}N_o + k_{d1}} \quad L_2 = \frac{k_{a2}N_o}{k_{a2}N_o + k_{d2}}$ $n_o = n_{o1} + n_{o2}$ $\eta_{12} = \frac{n_{o1}}{n_o}\cdot L_1 + \left(1 - \frac{n_{o1}}{n_o}\right)\cdot L_2$
b	$N + n_1 \overset{k_1}{\rightarrow} x_1$ $N + n_2 \overset{k_2}{\rightarrow} x_2$	$x(t) = x_1(t) + x_2(t) = n_o\cdot\left(1 - \frac{n_1}{n_o}e^{-k_1N_ot} - \left(1 - \frac{n_1}{n_o}\right)e^{-k_2N_ot}\right)$ $n_o = n_{o1} + n_{o2}$
c	$N + n_a \underset{k_d}{\overset{k_a}{\rightleftarrows}} x_a$ $N + n_i \overset{k_i}{\rightarrow} x_i$	$x(t) = x_a(t) + x_i(t) = n_o\cdot\eta\left[1 - \frac{n_a}{n_o}\cdot\frac{1}{\eta}\cdot L\cdot e^{-\kappa t} - \left(1 - \frac{n_a}{n_o}\right)\cdot\frac{1}{\eta}\cdot e^{-k_iN_ot}\right]$ $\kappa = k_aN_o + k_d$ $L = \frac{k_aN_o}{k_aN_o + k_d} \quad \eta = \frac{n_{oa}}{n_o}\cdot L + \left(1 - \frac{n_{oa}}{n_o}\right)$ $n_o = n_{oa} + n_{oi}$
d	$N + n \underset{k_d}{\overset{k_a}{\rightleftarrows}} z \overset{k_i}{\rightarrow} y$	$x(t) = n_o\left[1 - \left(\frac{\lambda_2(1-\lambda_1)}{\lambda_2 - \lambda_1}\right)e^{-\lambda_1k_it} - \left(\frac{\lambda_1(\lambda_2 - 1)}{\lambda_2 - \lambda_1}\right)e^{-\lambda_2k_it}\right]$ $\lambda_1 = \frac{1}{2k_i}[(k_aN_o + k_d + k_i) - \sqrt{(k_aN_o + k_d + k_i)^2 - 4k_ik_aN_o}]$ $\lambda_2 = \frac{1}{2k_i}[(k_aN_o + k_d + k_i) + \sqrt{(k_aN_o + k_d + k_i)^2 - 4k_ik_aN_o}]$ $z(t) = n_o\frac{\lambda_1\lambda_2}{\lambda_2 - \lambda_1}[e^{-\lambda_1k_it} - e^{-\lambda_2k_it}]$

cence decrease as a function of incubation time preceding the triggering of dissociation. This is shown in Fig. 6. It can be seen that the amount of particles released by the cells, increased and plateaued paralleling the establishment of an equilibrium. At the plateau, the fraction of the initially bound particles is close to 0.4. This demonstrated the existence of a reversibly bound fraction in agreement with a binding model of type **c** with two independent classes of binding sites, one populated through equilibrium, the other one through an irreversible binding. We then adjusted our data (Figs. 4 and 6) to the analytical expression provided by this model (see in model **c,** Table 1). The rate constant values extracted from the fit are given in Table 2. The fraction of reversible binding sites was found to be equal to 0.35 ± 0.1 by fitting the association data. This was quite close to what was expected on the basis of the dissociation experiments. This was also the case for the value of k_d that was found equal to $8.7 \times 10^{-3}\ s^{-1}$ by fitting the dissociation curve in Fig. 5 and equal to $6.2 \times 10^{-3}\ s^{-1}$ by fitting the association kinetics (Fig. 4 and Table 2).

Serum dependence of the binding

The association of the cationic particles with the cells was also analyzed in the presence of 10% fetal calf serum in the medium to evaluate the role of proteins in the binding. The total amount of bound particles was not significantly affected by the presence of proteins. However, the analysis of the kinetics according to model **c** revealed that the main effect of proteins consisted of an increase of the value of k_d, the reversible dissociation constant. The values of the rate constants are shown in Table 2. Values of k_a and k_i were indeed within the same range of values as the corresponding values obtained in the absence of proteins.

Temperature dependence

We were first interested in determining how the mechanism of binding was affected when the temperature was increased, particularly at 37°C. However, temperature elevation induced significant particle aggregation, as seen in the

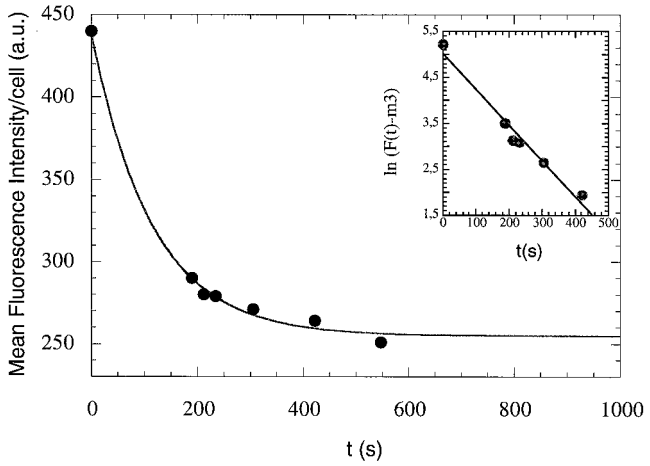

FIGURE 5 Analysis of the kinetics of the dissociation profile. J774 cells were incubated with calcein-loaded cationic particles (2×10^{14} particles/l) at 4°C, without fetal calf serum. Data were recorded on the sample taken up at time $t = 2200$ s. This time is considered here as time $t = 0$. The full line represents the fit obtained according to the analytical expression $y = m_1 e^{-m_2 x} + m_3$. The parameter m_3 gives the value of the dissociation constant k_d.

cytometry scattering plots (Fig. 7 *A*). This aggregation became significant above 15°C and seemed to grow cooperatively (Fig. 7 *B*). This phenomenon severely altered the binding curves and prevented the determination of the rate constants. The binding plots recorded at 25°C and 37°C (Fig. 8) suggested that the aggregates bound to the cells, but with different characteristics. We observed that, in the presence of these aggregates, binding was disturbed by stirring, suggesting that aggregates were weakly bound to the cells. Fluorescence microscopy observations confirmed this hypothesis showing large fluorescent structures on the surface

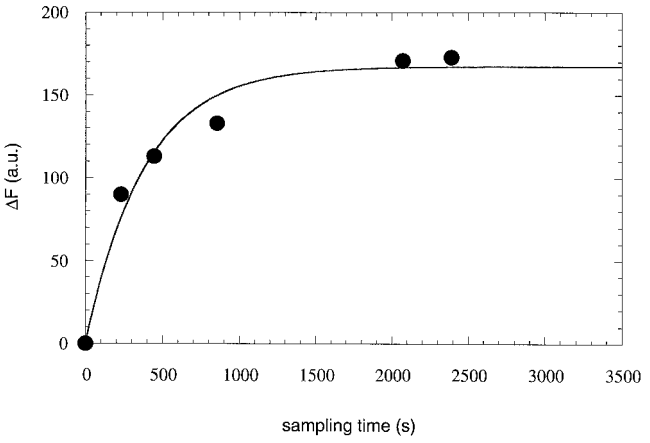

FIGURE 6 Evolution of the dissociation amplitude with pre-incubation time. The amount of fluorescence (mean fluorescence per cell) released upon washing has been plotted as a function of the incubation time t elapsed before the sample was taken. Same experimental conditions as in Fig. 5.

of the cells after 2 h of incubation at 37°C (data not shown). These structures were not endocytosed by the cells, as the fluorescence always remained at the periphery. To check the endocytosis capabilities of our cell line, we performed experiments with FITC-transferrin. This protein possesses specific receptors on the cell surface. Its endocytosis has been extensively described and was expected to occur rapidly at 37°C. Cells were first incubated at 4°C for 30 min, sampled for microscope observation, and incubated at 37°C for 30 min more. FITC-transferrin was totally internalized after 30 min at 37°C. This indicated that the cell metabolism was active under the conditions we used for the cationic particle experiments.

Positive charge density-dependence

The role of the charge density in the binding process was also investigated. MLVs containing 5% and 20% cationic lipids (DOTAP) were prepared to allow the comparison with previous results obtained with 10% cationic lipids. The binding curves are shown in Fig. 9. The rate constant values obtained are given in Table 2. When only 5% of cationic lipids are present, the binding is significantly reduced. The value of k_d appeared to be significantly higher than the one obtained with 10 or 20% DOTAP. Meanwhile, the k_a value was slightly lower and k_i was conserved. The results obtained with 20% DOTAP were very close to those obtained with 10% DOTAP.

DISCUSSION AND CONCLUSIONS

The mechanisms by which cationic particles interact with cells are not well understood. The structures involved in the interaction can reasonably be hypothesized to be of anionic nature and the binding process is expected to be primarily governed by electrostatic interactions, all the more as the cell surface exhibits substantial densities of negative charges. Actually, the extracellular matrix consists chiefly of sulfated glycosaminoglycans and polysaccharide acids, which form a hydrophilic negatively charged gel over the cell membrane. Integral membrane glycoproteins, most often bearing sialic acid residues, and membrane lipids also contribute to the negative charge density of the cell surface. Our results strongly supported this simple view because no measurable interaction was detected, under our experimental conditions, between particles devoid of net positive charges and cells. This absence of significant interaction between neutral particles and cells in vitro had already been evidenced with liposomes in the early work of Leserman et al. (1981) where no biological effect was detected with untargeted liposomes made of neutral lipids. Other authors have also found low but measurable interactions between cells and neutral particles (Miller et al., 1998; Lee et al., 1993). Aside from the strong cell-liposome interaction due

TABLE 2 Rate constant values for the binding of cationic spherulites to J774 cells at 4°C

Experimental Conditions		Rate Constants		
% DOTAP	Proteins*	k_aN_o (s^{-1})	k_d (s^{-1})	k_iN_o (s^{-1})
10	−	$(1.0 \pm 0.5) \times 10^{-1}$	$(6.2 \pm 3) \times 10^{-3}$	$(1.8 \pm 0.5) \times 10^{-3}$
10	+	$(0.37 \pm 0.5) \times 10^{-1}$	$(5.7 \pm 2) \times 10^{-2}$	$(1.5 \pm 0.5) \times 10^{-3}$
5	−	$(0.18 \pm 0.5) \times 10^{-1}$	$(1.1 \pm 0.3) \times 10^{-1}$	$(1.8 \pm 0.5) \times 10^{-3}$
20	−	$(0.65 \pm 0.5) \times 10^{-1}$	$(9.6 \pm 3) \times 10^{-3}$	$(2 \pm 0.5) \times 10^{-3}$

N_o is the total particle concentration of the experiment. Here $N_o = 2 \times 10^{14}$ part./l or 3.3×10^{-10} M (moles of particles per litre). k_aN_o and k_iN_o are apparent rate constants.
*10% fetal calf serum.

the presence of net positive charges on the latter, the most significant finding in our work was that the binding to the cell surface, in the absence of any internalization, occurred by two independent pathways. Up to now, the uptake of colloids by the cell has been described as the occupation of one class of binding sites according to a thermodynamic equilibrium, followed by the internalization of the bound particle into the cell. This binding scheme was proposed by several groups in quantitative analysis of liposome capture by cells (Kirpotin et al., 1997; Lee et al., 1993; Straubinger et al., 1990). We reached here a different description of the association of such colloids with the cell. This could result from the particle characteristics—ours were cationic—but also from the different technical approach that we have used: 1) kinetic data were acquired by flow cytometry in the absence of the perturbation from equilibrium that is induced by washing steps. 2) We have examined the particle dissociation characteristics, and 3) we have also worked in the absence of endocytosis. We now propose a model involving two classes of binding sites on the cell surface. One binding mode consisted of a thermodynamic equilibrium characterized by an affinity constant K, the value of which is given by the ratio of the rate constants k_a and k_d. At 4°C, in the absence of proteins, the affinity constant was equal to 5×10^{10} M^{-1}. This accounts for the binding of a spherulite containing 10% DOTAP to one cellular binding site. This is to be compared with the affinity constant calculated for the binding of a free Fab′ fragment from a 4D5 antibody to its cell surface receptor, which was found equal to 5×10^7 M^{-1} (Sarup et al., 1991) and reached 2×10^8 M^{-1} for the whole antibody. Liposomes made of phosphatidylcholine, cholesterol, and the negatively charged phosphatidylserine have been found to bind to J774 cells with an affinity constant equal to 10^9 M^{-1} (Lee et al., 1993). Neutral lipo-

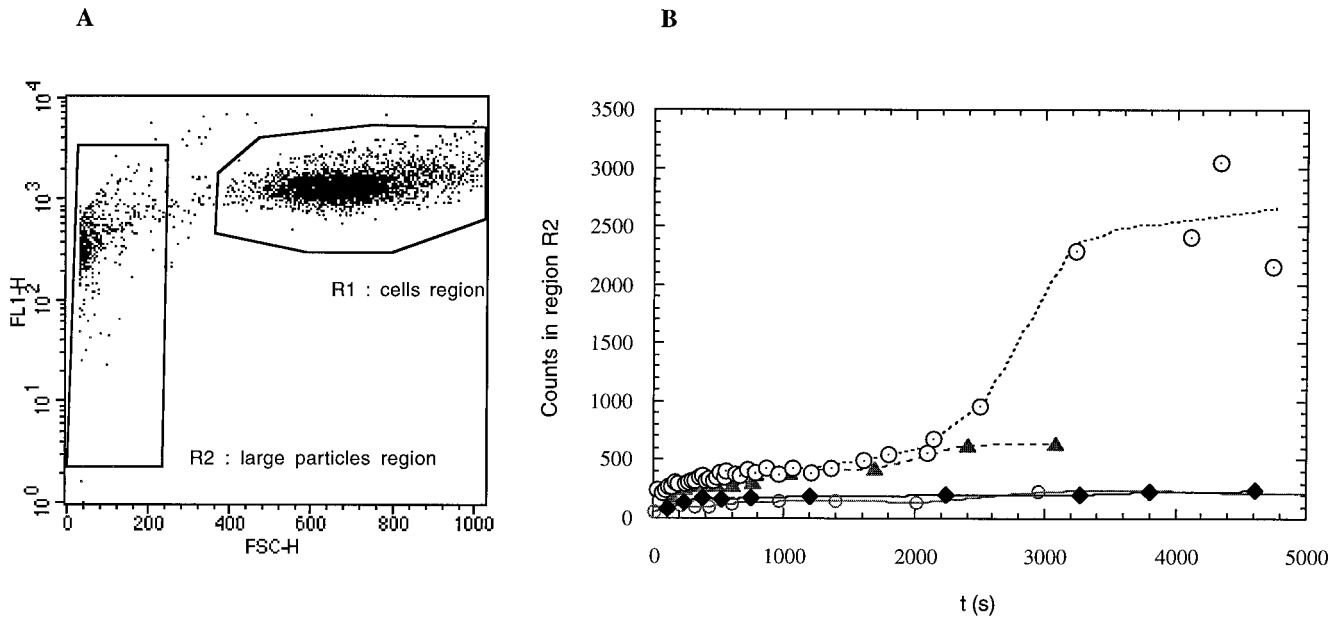

FIGURE 7 Particle aggregation at 37°C. (*A*) shows the distribution of the mean fluorescence per event together with the small angle scattering (FSC) measured on J774 cell samples incubated 2 h at 37°C with 2×10^{14} particles/ml. Gate R1 defines the (FL1; FSC) couples of values characterizing the cell population. Gate R2, at low FSC values, comprises small size events, i.e., events having a diameter ~1 μm. This gate comprises particle aggregates. (*B*) shows the population contained in gate R2 as incubation time elapses at different temperatures.

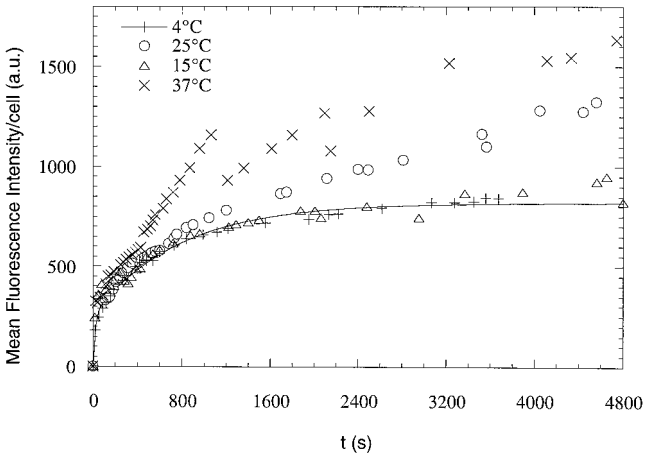

FIGURE 8 Kinetics of cationic particles capture by J774 cells at different temperatures. Same experimental conditions as in Fig. 4 except that measurements have been performed at 4°C (+); 15°C (Δ); 25°C (○) and 37°C (×).

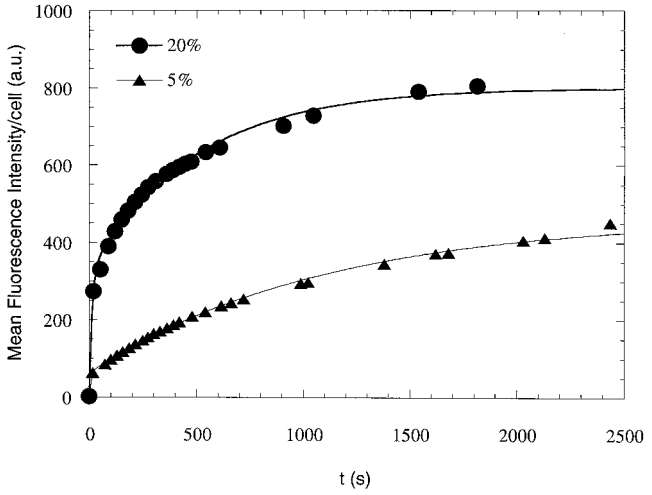

FIGURE 9 Kinetics of capture by J774 cells of particles containing 5% (●) and 20% (△) DOTAP. Experimental conditions same as in Fig. 4.

somes covered with 0.5% anti-HeR2 Fab fragments were shown to bind specific receptor-bearing cells with a 7×10^9 M^{-1} affinity constant (Kirpotin et al., 1997). Ellens et al. (1990) obtained an affinity constant equal to 7×10^{10} M^{-1} for binding to glycophorin-containing liposomes to cells expressing influenza hemagglutinin on their surfaces. The association of biotin with avidin gives a well-known example of a very high-affinity complex. The affinity constant has been found of the order of 10^{15} M^{-1} (Bayer and Wilchek, 1980). Thus, the affinity constant that we have found for the binding of MLVs bearing 10% positive charges over J774 cells stands within the range of affinities obtained for synthetic particles specifically targeted with physiologic ligands. The value of the measured affinity constant reflects both the intrinsic affinity of the ligand for its receptor and the valency of the particle (the number of ligands per particle) together with the efficacy of the valency (how many ligands available on the same particle are able to interact at the same time). It has been shown for targeted particles that the valency of the particle was a determining parameter of the binding. Schaffer and Lauffenburger (1998) found an optimal valency of 15 for molecular conjugates targeted to fibroblasts with epidermal growth factor. Similarly, we found with cationic particles that the affinity constant drastically dropped when the fraction of cationic lipids was reduced from 10% to 5%, whereas it remained practically unchanged when the fraction of cationic lipids was increased from 10% to 20%. Considering a mean-square surface of 64 $Å^2$ per lipid headgroup and a mean particle diameter of 200 nm, we can estimate that the number of positive charges per particle made of 10% DOTAP is approximately equal to 2×10^4. It can then be easily imagined that several cationic molecules are involved in one link.

It should be noticed that, within the range of affinities expressed by both cationic particles and liposomes targeted with physiologic ligands, the fraction of free particles compared to bound particles for a given cell concentration will be highly dependent on the number of receptors per cell. In the present case, because the free fraction (N) was always high, it can be estimated that the number of sites over a cell should be of the order of a few hundreds. Some authors have calculated receptor numbers up to 10^5 per cell (Schaffer and Lauffenburger, 1998). This will be an important parameter to consider in the development of drug delivery vehicles because the presence of a significant fraction of free vesicles is to be avoided.

Besides the thermodynamic equilibrium, cationic particles were shown to bind to cell surface irreversibly, with an apparent rate constant $k_i N_o$ equal to 1.8×10^{-3} s^{-1}. This could also be seen and understood as a binding equilibrium characterized by an infinite affinity constant. The irreversible binding appeared to be two orders of magnitude slower than the equilibrium, indicating that, although strong, this association of the particles to the cells had a much lower probability of occurring than the one governed by the equilibrium. Thus, two distinct classes of binding sites exist for cationic particles. Both captures were driven by electrostatic interactions because they were not observed in the absence of charges. The energy of adhesion can be calculated from the value of the affinity constant. It was found close to 65 kT per site, which is relatively high, if one considers that an ion pair with the two ions separated by a distance of 7 Å in water has an energy of interaction equal to 1 kT. This suggests that a significant number of electrostatic links should be involved in this interaction. At our current level of understanding, the irreversible binding site can be assumed to be either of a totally different nature or involving a much higher number of links because, for instance, it would be

located in an area of high concentration of negative charges. From the kinetic point of view we have found, for 10% DOTAP-containing MLVs, binding rate constants equal to $3 \times 10^8\ M^{-1}\ s^{-1}$ and $4.5 \times 10^6\ M^{-1}\ s^{-1}$ for the reversible and irreversible binding sites, respectively. These rate constant values are one and three orders of magnitude lower than values characterizing diffusion-controlled processes, respectively. This indicated the existence of high potential barriers for the binding of these particles to the cells. Other authors have found rate constant values significantly higher than ours. For instance, Nir et al. (1986) have determined a rate constant $k_a = (1.9–3.5) \times 10^9\ M^{-1}\ s^{-1}$ for the binding of Sendai virus to ghost erythrocytes. Lee et al. (1993) have obtained a rate constant $k_a = (0.6–3.7) \times 10^9\ M^{-1}\ s^{-1}$ for the binding of negatively charged liposomes to J774 cells. In the case of Sendai virus binding, the high-affinity constant value has been attributed to the existence of spikes on the virus envelope, which could favor the close approach of the viral particle and lower the potential barrier. In the case of negatively charged liposomes, the reason for having a high association rate constant is less clear. The authors have treated the binding with a mass action law applied to one class of sites that were internalized in a second step. The model that we propose here is rather different, because we consider two classes of independent binding sites on the cell surface. Both were detected at 4°C. This could be also a reason why our values are lower. However, Lee et al. did not find a significant difference between the association rate constants that they obtained at 4 and 37°C in the presence of endocytosis inhibitors. The respective values of the rate constants that we have obtained for the two types of sites suggest that the irreversible site has a reduced accessibility, inducing a high activation barrier. This could be the case for a binding site located at the membrane level, close to the lipid bilayer, whose access could be hindered by the network of the extracellular matrix polymers. In contrast, the lower-affinity binding site was populated with a two-orders-of-magnitude higher rate constant, suggesting that it could reside at the extracellular matrix level itself. Mislick and Baldeschwieler (1996) have in fact demonstrated a role for proteoglycans, an extracellular matrix component, in cation-mediated gene transfer efficiency. Additional experiments, using enzymes that inhibit the expression of the extracellular matrix components, would help to strengthen our hypothesis. In this work we have developed the tools necessary to deepen the understanding of the binding mechanism by investigating how each binding component can be modulated. The absence of endocytosis in this system was rather surprising. One reason for this could lie in the aggregation of the particles examined when the temperature was raised. This resulted in the binding of large entities that the cell may not have been able to internalize. We are currently working to solve this problem and obtain endocytosis of individual particles at 37°C. It would be, indeed, of primary interest to gain further insight in the particle capture process, to understand if the cell processes in a similar or distinct manner the particles bound on the two different classes of binding sites.

APPENDIX

Considering a simple reaction as:

$$N + n \xrightarrow{k} x$$

We obtain a kinetic equation describing the formation of x, which is:

$$\frac{dx}{dt} = k(N_o - x)(n_o - x)$$

with N_o and n_o being the initial concentrations of N and n, respectively. Assuming that $N_o \gg x$, we have the simple linear equation

$$\frac{dx}{dt} = (kN_o)x + (kN_o n_o)$$

The solution is

$$x(t) = n_o(1 - e^{-kN_o t})$$

Similarly, for an equilibrium

$$N + n \underset{k_d}{\overset{k_a}{\rightleftarrows}} x$$

we have

$$\frac{dx}{dt} = k_a N_o(n_o - x) - k_d x$$

and

$$x(t) = \frac{k_a N_o}{k_a N_o + k_d}(1 - e^{-(k_a N_o + k_d)t})$$

When these processes take place at the same time but independently, the expression of $x(t)$ is obtained simply by calculating the sum of the products formed by each process.

These processes can also be combined as

$$N + n \underset{k_d}{\overset{k_a}{\rightleftarrows}} z \xrightarrow{k_i} y$$

with

$$x(t) = z(t) + y(t)$$

then

$$\frac{d(x - y)}{dt} = k_a N_o(n_o - x) - (k_d + k_i)(x - y)$$

$$\frac{dy}{dt} = k_i(x - y)$$

After adequate variable changes and integration, we obtain:

$$x(t) = n_o\left[1 + \left(\frac{\lambda_2(\lambda_1 - 1)}{\lambda_2 - \lambda_1}\right)e^{-\lambda_1 k_i t} - \left(\frac{\lambda_1(\lambda_2 - 1)}{\lambda_2 - \lambda_1}\right)e^{-\lambda_2 k_i t}\right]$$

with

$$\lambda_1 = \frac{1}{2k_i}\left[(k_a N_o + k_d + k_i) - \sqrt{(k_a N_o + k_d + k_i)^2 - 4k_i k_a N_o}\right]$$

$$\lambda_2 = \frac{1}{2k_i}\left[(k_a N_o + k_d + k_i) + \sqrt{(k_a N_o + k_d + k_i)^2 - 4k_i k_a N_o}\right]$$

and

$$z(t) = n_o\frac{\lambda_1\lambda_2}{\lambda_2 - \lambda_1}\left[e^{-\lambda_1 k_i t} - e^{-\lambda_2 k_i t}\right]$$

We thank Prof. C. Coulon for the benefit of his expertise in the field of data analysis and Prof. J. Bibette and Dr. P. Poulin for helpful discussions.

REFERENCES

Allen, T. M., and C. Hansen. 1991. Pharmacokinetics of stealth versus conventional liposomes: effect of dose. *Biochim. Biophys. Acta.* 1068: 133–141.

Allen, T. M., T. Mehra, C. Hansen, and Y. C. Chin. 1992. Stealth liposomes: an improved sustained release system for 1-beta-D-arabinofuranosylcytosine. *Cancer Res.* 52:2431–2439.

Allen, T. M., P. Williamson, and R. A. Schlegel. 1988. Phosphatidylserine as a determinant of reticuloendothelial recognition of liposome models of the erythrocyte surface. *Proc. Natl. Acad. Sci. USA.* 85:8067–8071.

Bayer, E. A., and M. Wilchek. 1980. The use of the avidin-biotin complex as a tool in molecular biology. *Methods Biochem. Anal.* 26:1–45.

Benita, S., and M. Y. Levy. 1993. Submicron emulsions as colloidal drug carriers for intravenous administration: comprehensive physicochemical characterization. *J. Pharm. Sci.* 11:1069–1079.

Bonté, F., and R. L. Juliano. 1986. Interactions of liposomes with serum proteins. *Chem. Phys. Lipid.* 40:359–372.

Boussif, O., M. A. Zanta, and J. P. Behr. 1996. Optimized galenics improve in vitro gene transfer with cationic molecules up to 1000-fold. *Gene Ther.* 3:1074–1080.

Diat, O., D. Roux, and F. Nallet. 1993. Effect of shear on lyotropic lamellar phase. *J. Phys. II.* 3:1427–1452.

Dufourcq, J., W. Neri, and N. Henry-Toulmé. 1998. Molecular assembling of DNA with amphipathic peptides. *FEBS Lett.* 421:7–11.

Ellens, H., J. Bentz, D. Mason, F. Zhang, and J. White. 1990. Fusion of influenza hemagglutinin-expressing fibroblasts with glycophorin-bearing liposomes: role of hemagglutinin surface density. *Biochemistry.* 29:9697–9707.

Erbacher, P., J. S. Remy, and J. P. Behr. 1999. Gene transfer with synthetic virus-like particles via the integrin-mediated endocytosis pathway. *Gene Ther.* 6:138–145.

Gao, X., and L. Huang. 1996. Potentiation of cationic liposome-mediated gene delivery by polycations. *Biochemistry.* 35:1027–1036.

Goren, D., A. T. Horowitz, S. Zalipsky, M. C. Woodle, Y. Yarden, and A. Gabizon. 1996. Targeting of stealth liposomes to erbB-2 (Her/2) receptor: in vitro and in vivo studies. *Br. J. Cancer.* 74:1749–1756.

Haensler, J., and F. C. Szoka. 1993. Polyamidoamine cascade polymers mediate efficient transfection of cells in culture. *Bioconjugate Chem.* 4:372–379.

Hallen, R. M. 1980. Colorimetric estimation of phospholipids in aqueous dispersions. *J. Biochem. Biophys. Methods.* 5:251–255.

Henry-Toulmé, N., M. Grouselle, and C. Ramasailles. 1995. Multidrug resistance bypass in cells exposed to doxorubicin-loaded nanospheres. Absence of endocytosis. *Biochem. Pharmacol.* 50:1135–1139.

Hofland, H. E., L. Shephard, and S. M. Sullivan. 1996. Formation of stable cationic lipid/DNA complexes for gene transfer. *Proc. Natl. Acad. Sci. USA.* 93:7305–7309.

Kamps, J. A., H. W. Morselt, and G. L. Scherphof. 1999. Uptake of liposomes containing phosphatidylserine by liver cells in vivo and by sinusoidal liver cells in primary culture: in vivo-in vitro differences. *Biochem. Biophys. Res. Commun.* 256:57–62.

Kendall, D. A., and R. C. McDonald. 1983. Characterization of a fluorescence assay to monitor changes in the aqueous volume of lipid vesicles. *Anal. Biochem.* 134:26–31.

Kirpotin, D., J. W. Park, S. Zalipsky, W-L. Li, P. Carter, C. C. Benz, and D. Papahadjopoulos. 1997. Sterically stabilized anti-HER2 immunoliposomes: design and targeting to human breast cancer cells in vitro. *Biochemistry.* 36:66–75.

Koltover, I., T. Salditt, J. O. Radler, and C. R. Safinya. 1998. An inverted hexagonal phase of cationic liposome-DNA complexes related to DNA release and delivery. *Science.* 281:78–81.

Kreuter, J. 1994. Drug targeting with nanoparticles. *Eur. J. Drug Metab. Pharmacokinet.* 19:253–256.

Lee, K-D., K. Hong, and D. Papahadjopoulos. 1992. Recognition of liposomes by cells: in vitro binding and endocytosis mediated by specific lipid headgroups and surface charge density. *Biochim. Biophys. Acta.* 1103:185–197.

Lee, K-D., S. Nir, and D. Papahadjopoulos. 1993. Quantitative analysis of liposome-cell interaction in vitro: rate constants of binding and endocytosis with suspension and adherent J774 cells and human monocytes. *Biochemistry.* 32:889–899.

Legendre, J. Y., and A. Supersaxo. 1995. Short-chain phospholipids enhance amphipathic peptide-mediated gene transfer. *Biochem. Biophys. Res. Commun.* 217:179–185.

Legendre, J. Y., and F. C. Szoka. 1993. Cyclic amphipathic peptide-DNA complexes mediate high-efficiency transfection of adherent mammalian cells. *Proc. Natl. Acad. Sci. USA.* 90:893–897.

Legendre, J. Y., A. Trzeciak, B. Bohrmann, U. Deuschle, E. Kitas, and A. Supersaxo. 1997. Dioleoylmelittin as a novel serum-insensitive reagent for efficient transfection of mammalian cells. *Bioconjugate Chem.* 8:57–63.

Leserman, L., P. Machy, and J. Barbet. 1981. Cell-specific drug transfer from liposomes bearing monoclonal antibodies. *Nature.* 293:226–228.

Meyer, O., D. Kirpotin, K. Hong, B. Sternberg, J. W. Park, M. C. Woodle, and D. Papahadjopoulos. 1998. Cationic liposomes coated with polyethylene glycol as carriers for oligonucleotides. *J. Biol. Chem.* 273: 15621–15627.

Miller, R. M., B. Bondurant, S. D. McLean, K. A. McGovern, and D. F. O'Brien. 1998. Liposome-cell interactions in vitro: effect of liposome surface charge on the binding and endocytosis of conventional and sterically stabilized liposomes. *Biochemistry.* 37:12875–12883.

Mislick, K. A., and J. D. Baldeschwieler. 1996. Evidence for the role of proteoglycans in cation-mediated gene transfer. *Proc. Natl. Acad. Sci. USA.* 92:12349–12354.

Nir, S., K. Klappe, and D. Hoekstra. 1986. Kinetics and extent of fusion between Sendai virus and erythrocytes ghosts: application of a mass action kinetic model. *Biochemistry.* 25:2155–2161.

Papahadjopoulos, D., T. M. Allen, A. Gabizon, E. Mayhew, K. Matthay, S. K. Huang, K-D. Lee, M. C. Woodle, D. D. Lasic, C. Redemann, and F. J. Martin. 1991. Sterically stabilized liposomes: improvements in pharmacokinetics and antitumor therapeutic efficacy. *Proc. Natl. Acad. Sci. USA.* 88:11460–11464.

Park, J. W., K. Hong, P. Carter, H. Asgari, L. Y. Guo, G. A. Keller, C. Wirth, R. Shalaby, C. Kotts, W. I. Wood, D. Papahadjopoulos, and C. C. Benz. 1995. Development of anti-p185HER2 immunoliposomes for cancer therapy. *Proc. Natl. Acad. Sci. USA.* 92:1327–1331.

Pires, P., S. Simões, S. Nir, R. Gaspar, N. Düzgünes, and M. C. Pedroso de

Lima. 1999. Interaction of cationic liposomes and their DNA complexes with monocytic leukemia cells. *Biochim. Biophys. Acta.* 1418:71–84.

Poste, G., and D. Papahadjopoulos. 1978. The influence of vesicle membrane properties on the interaction of lipid vesicles with cultured cells. *Ann. NY Acad. Sci.* 308:164–184.

Roerdink, F., N. M. Wassef, E. C. Richardson, and C. R. Alving. 1983. Effects of negatively charged lipids on phagocytosis of liposomes opsonized by complement. *Biochim. Biophys. Acta.* 734:33–39.

Sarup, J. C., R. M. Johnson, K. L. King, B. M. Fendly, M. T. Lipari, M. A. Napier, A. Ullrich, and H. M. Shepard. 1991. Characterization of an anti-p185HER2 monoclonal antibody that stimulates receptor function and inhibits tumor cell growth. *Growth Regul.* 37:72–82.

Schaffer, D. V., and D. A. Lauffenburger. 1998. Optimization of cell surface binding enhances efficiency and specificity of molecular conjugate gene delivery. *J. Biol. Chem.* 43:28004–28009.

Scherphof, G., J. Damen, and D. Hoekstra. 1981. Interactions of liposomes with plasma proteins and components of the immune system. *In* Liposomes: From Physical Structure to Therapeutic Applications. C. G. Knight, editor. Elsevier, Amsterdam. 299–322.

Schwartz, B., C. Benoist, B. Abdallah, D. Scherman, J. P. Behr, and B. A. Demeneix. 1995. Lipospermine-based gene transfer into the newborn mouse brain is optimized by a low lipospermine/DNA charge ratio. *Hum. Gene Ther.* 6:1515–1524.

Straubinger, M. R., D. Papahadjopoulos, and H. Keelung. 1990. Endocytosis and intracellular fate of liposomes using pyranine as a probe. *Biochemistry.* 29:4929–4939.

Wadhwa, M. S., W. T. Collard, R. C. Adami, D. L. McKenzie, and K. G. Rice. 1997. Peptide-mediated gene delivery: influence of peptide structure on gene expression. *Bioconjugate Chem.* 8:81–88.

Woodle, M. C., and D. D. Lasic. 1992. Sterically stabilized liposomes. *Biochim. Biophys. Acta.* 1113:171–199.

Yang, J. P., and L. Huang. 1998. Time-dependent maturation of cationic liposome-DNA complex for serum resistance. *Gene Ther.* 5:380–387.